Ultrasonics - Sonochemistry 66 (2020) 105093

Contents lists available at ScienceDirect

Ultrasonics - Sonochemistry

journal homepage: www.elsevier.com/locate/ultson

# Ultrasonic-assisted eggshell extract-mediated polymorphic transformation of calcium carbonate

Sevgi Polat*, Perviz Sayan

*Department of Chemical Engineering, Faculty of Engineering, Marmara University, 34722 İstanbul, Turkey*

ARTICLE INFO

*Keywords:*
Calcium carbonate
Ultrasonic irradiation
Eggshell extract
Box–Behnken design, Polymorphs
Vaterite

ABSTRACT

This study aimed to evaluate the combined effects of eggshell extract and ultrasonic irradiation on the polymorphic transformation of calcium carbonate ($CaCO_3$). In this context, XRD, Raman spectroscopy, SEM, AFM, TGA-FTIR, BET, and zeta potential analysis were used to identify and characterize the different polymorphs of $CaCO_3$ obtained in the absence and presence of eggshell extract in the media with and without ultrasonic irradiation. The morphology and polymorphic nature of the $CaCO_3$ crystals were observed to change, which indicated that the eggshell extract and ultrasonication influenced the structure and crystallization of $CaCO_3$. The structural analysis results indicated that the addition of eggshell extract to the media resulted in the full transformation of calcite to the vaterite polymorph. The results also showed that ultrasonic irradiation had a more significant influence on the BET specific surface area of the crystals compared to the eggshell extract media. Furthermore, a Box–Behnken design with response surface methodology was employed to determine the optimal operating conditions for $CaCO_3$ crystallization. The effects of stirring rate, extract concentration, and ultrasonic power on the BET surface area were investigated. The results show that the data sufficiently fit the second-order polynomial model. Understanding the eggshell extract-mediated polymorphic transformation with ultrasonic irradiation obtained in this study makes it possible to control the polymorphic formation and modify the product characteristics.

## 1. Introduction

Calcium carbonate ($CaCO_3$), a very important mineral, has attracted a significant interest in recent decades owing to its wide-ranging industrial applications and importance in biomineralization research. As a typical biomineral, it is abundant in both organisms and nature [1–4]. It is well known that $CaCO_3$ can be found in three anhydrous polymorphs: vaterite, aragonite, and calcite, with hexagonal, orthorhombic, and rhombohedral structures, respectively, listed in order of increasing thermodynamic stability [5,6]. Calcite is important in the cement and metallurgy industries [7], while aragonite is typically used as a filler for biomedical materials and in new composite materials [8]. Vaterite is the least abundant polymorph in nature, but it is a strong candidate for practical biomedical applications owing to its high specific surface area, good water solubility and dispersion, and lower density compared to the other two crystal polymorphs [9]. Parakhonskiy et al. [10] reported the use of porous spherical vaterite particles for controlled release of drugs whilst Schröder et al. [11] investigated the use of vaterite nanoparticles for the treatment of bone defects and degenerative bone diseases. Therefore, the production of vaterite with various structures, morphologies, and surface properties by various methods is of great importance.

It is well known that organic and ionic additives play crucial roles in modifying and/or controlling the crystallization of the three polymorphs of $CaCO_3$. Some examples of the additives studied to date include amino acids [12], polyelectrolytes [13–15], polypeptides [16], polycarboxylic acids [17], copolymers [18], vitamins [19], and foreign ions [20,21]. In this study, eggshell extract, which is important for biomineralization and has studied extensively, was selected as an additive. The polymorphs of $CaCO_3$ can be modified by ultrasonic treatment and suitable additives. The effects of ultrasonic irradiation on $CaCO_3$ polymorphism are not yet fully understood, but literature reports indicate that ultrasonication enhances the spontaneous precipitation of $CaCO_3$ [22,23]. Moreover, there are few reports in the literature on the combined effects of additives and ultrasonic irradiation on $CaCO_3$ polymorphism.

Thus, the present study was conducted to investigate the polymorphic transformation of calcite to vaterite with and without ultrasonic irradiation in the presence and absence of eggshell extract. The effects of the ultrasonication power on the particle size, shape, and

* Corresponding author.
*E-mail address:* sevgi.polat@marmara.edu.tr (S. Polat).

https://doi.org/10.1016/j.ultsonch.2020.105093
Received 9 February 2020; Received in revised form 11 March 2020; Accepted 23 March 2020
Available online 25 March 2020
1350-4177/ 

surface area were also studied. The effects of eggshell extract on $CaCO_3$ polymorphs were determined through structural and morphological analysis, the results of which will contribute to the understanding of the growth of the different $CaCO_3$ polymorphs in the presence of eggshell extract with ultrasonication. Furthermore, experimental design was applied to determine what effects the process variables of stirring rate, extract concentration, and ultrasonic power had on the $CaCO_3$ crystallization. The novel aspect of this work is the preliminary investigation of the variables that affect the polymorphic transformation of $CaCO_3$ and any possible interactions using a suitable experimental design in order to find the optimal conditions to produce the greatest BET specific surface area. We believe that the detailed investigation of the effects of interactions between the process variables on $CaCO_3$ crystallization will provide invaluable information for application in a diverse range of industries. Moreover, the characterization and process optimization results reported in this work will provide useful guidance for controlling the $CaCO_3$ surface area in future studies.

## 2. Experimental method

Pure powdered calcium chloride dihydrate ($CaCl_2{\cdot}2H_2O$, Merck), sodium carbonate ($Na_2CO_3$, Merck), and distilled water were used in all experiments.

The experiments were carried out in a 1.5-L stainless-steel crystallizer with a thin wall, as illustrated in Fig. 1. To apply ultrasonic irradiation to the crystallizer, the crystallizer was placed into a specially designed ultrasonic water bath. This specially designed water bath reduces the cavitation effect observed in immersed ultrasonic probes, allowing the local ultrasonic effect to be homogeneously applied throughout the crystallizer.

As shown in Fig. 1, the water bath contained four ultrasonic horns, which were used as the ultrasonic source. The ultrasonic horns were operated at a frequency of 20 kHz and the experiments were performed at ultrasonic powers of 90 W and 180 W. The temperature was controlled with a sensitivity of 30 ± 0.1 °C using a thermostat connected to a cooling coil produced out of stainless-steel placed in the water bath. The crystallization media was stirred at a constant rate of 300 rpm using a propeller blade connected to a mechanical stirrer. $CaCl_2{\cdot}2H_2O$ and $Na_2CO_3$ were used as the reactants to produce $CaCO_3$.

At the beginning of the experiments, 500 mL of 0.2 M calcium chloride solution was put into the crystallizer and left to reach thermal equilibrium. Afterwards, 500 mL of 0.2 M sodium carbonate solution was fed into the crystallizer at a rate of 4 mL/min using a peristaltic pump. The pH of the solution was maintained at 8.5 by a pH control unit with a peristaltic pump dispensing sodium hydroxide solution.

The eggshell extract was prepared by separating the eggshells from the membrane and then boiling them in distilled water for half an hour to remove any impurities. The eggshells were then dried, ground, and sieved. The sieved eggshell was then characterized using XRD and SEM/EDX analysis to identify the structures and surface morphology. The XRD results showed that the main component of the eggshell sample was $CaCO_3$, as seen in Fig. 2(a). The SEM image in Fig. 2(b) shows that the surface of the sample is generally composed of irregularly shaped particles with nearly uniform size. According to the corresponding EDX spectrum, (Fig. 2(c)) mainly C, O, Na, Mg, Ca, and Si were detected on the surface of the eggshell sample.

The ground eggshells were dissolved in a 10% HCl solution. This mixture was first passed through a Whatman Blue Ribbon filter paper and then through a membrane filter with a nominal pore size of 0.45 μm. The obtained extract was then used in the polymorphism experiments by being added to the calcium chloride solution at the beginning of the crystallization at a ratio of 2.5 wt%. The pH of the solution was set at 8.5 at the beginning of the experiments, and then reactant feeding commenced.

This study also examined the polymorphic transformation of $CaCO_3$ in the presence of ultrasonic irradiation. For this purpose, two different ultrasonic powers of 90 W and 180 W were utilized. The experiments were carried out firstly in pure medium, then in the presence of the eggshell extract in the medium with and without ultrasonic irradiation. During the experiments, the ultrasonic irradiation was applied continuously. At the end of the experiments, the samples were withdrawn from the crystallizer, quickly filtered, and washed with distilled water, then the solid phase was dried and analyzed.

The crystal structure was characterized by X-ray diffractometer (Bruker D2 Phaser Table-top Diffractometer) with Cu Kα radiation (λ = 1.542 Å) within a 2θ range of 10° to 80°. Further structural analysis was performed using a Raman microscope (Renishaw InVia Reflex). Fourier transform infrared spectroscopy (FTIR; Shimadzu IR Affinity-1) was used to provide information on the polymorphic change and to confirm the adsorption of the eggshell extract on the surface of the $CaCO_3$. The spectra were recorded in a scanning range of 400 to 4000 $cm^{-1}$ at room temperature. The morphology of the $CaCO_3$ was

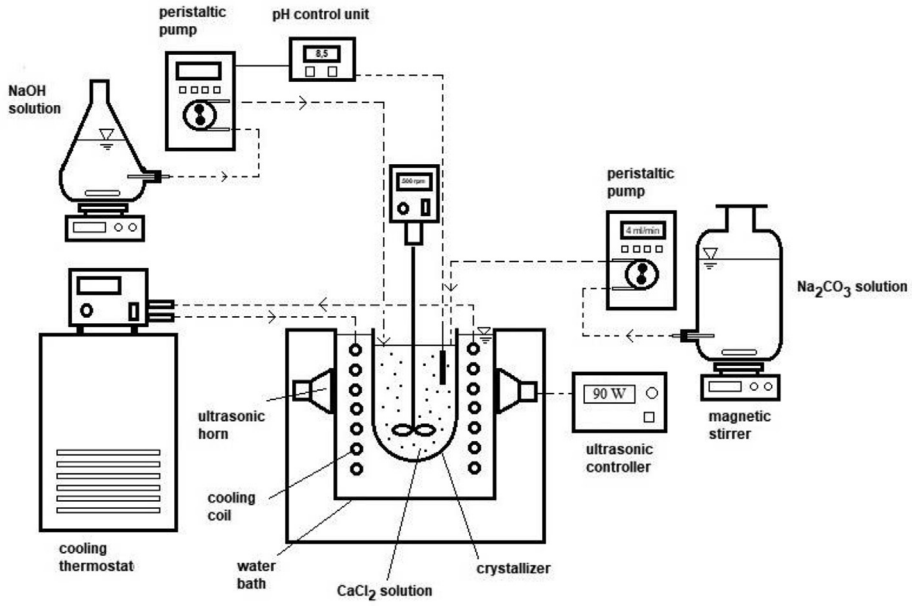


**Fig. 1.** The experimental setup.

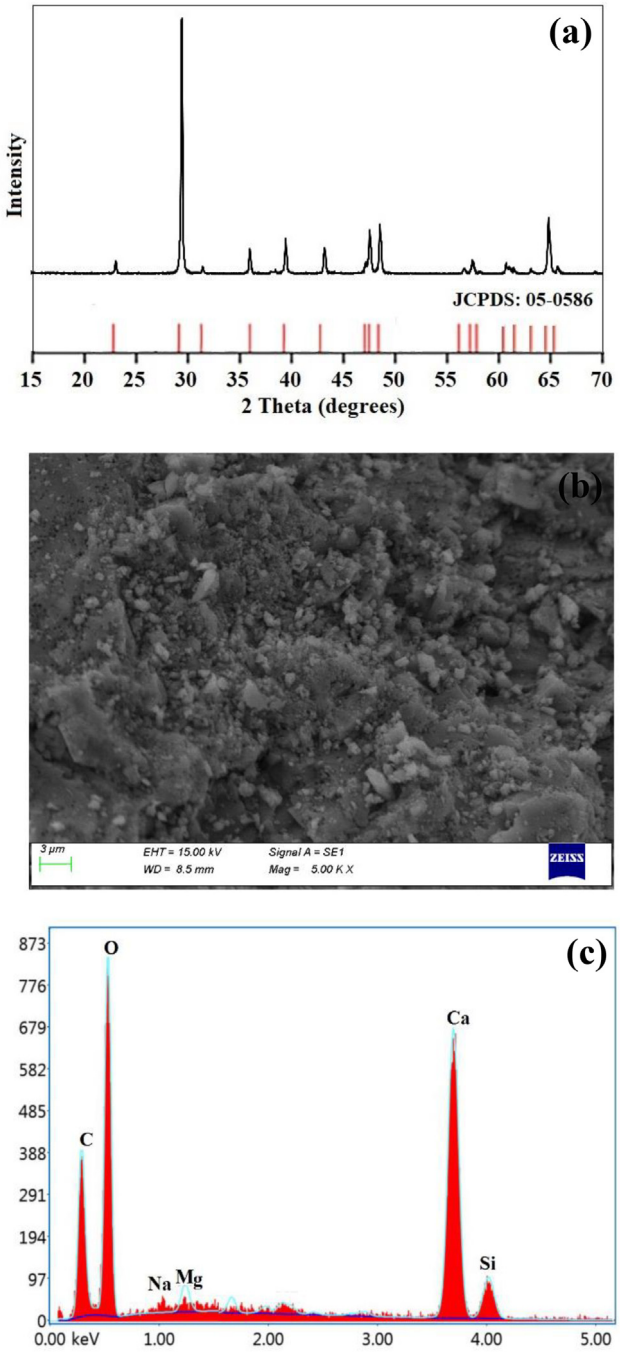


**Fig. 2.** (a) XRD, (b) SEM and (c) EDX results of eggshell sample.

investigated by scanning electron microscopy and energy-dispersive X-ray spectroscopy (SEM/EDX; Zeiss EVO LS 10) as well as atomic force microscopy (AFM). Thermal analysis of the $CaCO_3$ was performed using a Netzsch STA 409. A sample of 20 ± 0.5 mg was placed in a crucible and heated over the temperature range of 25 to 1000 °C at a heating rate of 20 °C/min. The Brunauer–Emmett–Teller (BET) specific surface area of the crystals was also analyzed using a Quantachrome Quadrosorb SI. In addition, TGA-FTIR analysis was performed to detect the gaseous species that evolved during thermal decomposition. This instrument comprised an FTIR spectrometer (PerkinElmer Spectrum 100) combined with a TGA system; and a heating rate of 20 °C/min was applied. Particle size and zeta potential measurements for the as-prepared crystals were obtained using a Malvern 2000 and a Malvern Zeta Sizer Nano Series Nano-ZS, respectively.

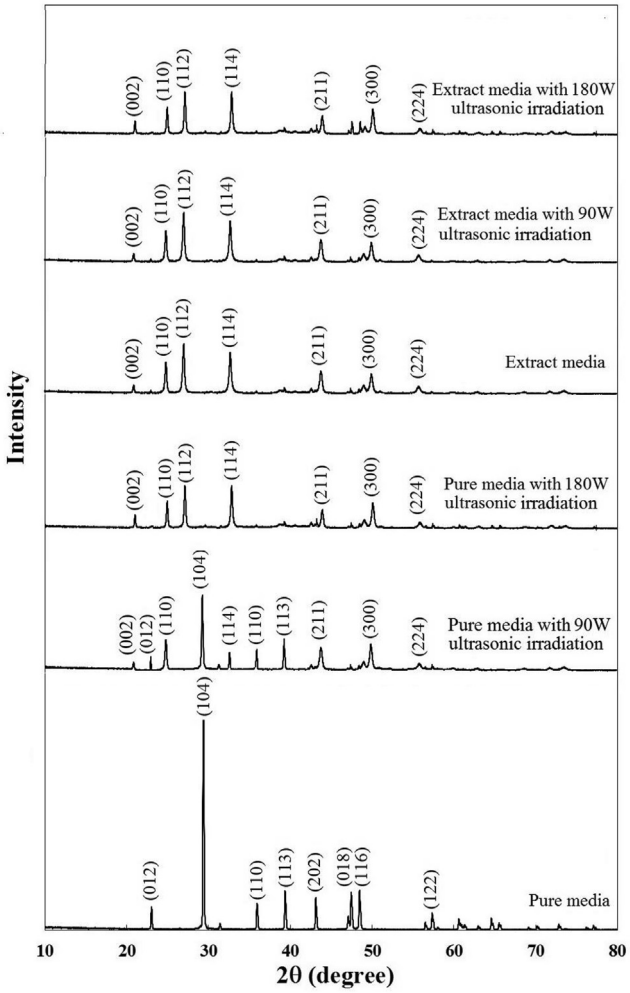


**Fig. 3.** XRD results for $CaCO_3$ crystals obtained in pure and eggshell extract-containing media with and without ultrasonication.

## 3. Results and discussion

### 3.1. XRD analysis

Fig. 3 shows the XRD patterns of the $CaCO_3$ crystals obtained in pure media and media containing the eggshell extract with and without ultrasonication. The XRD pattern for the sample obtained in pure, unsonicated media indicates that that calcite (JCPDS: 05-0586) was the only crystalline phase produced.

The XRD pattern for the sample produced with 90 W ultrasonic irradiation without eggshell extract revealed the presence of another crystalline phase: vaterite (JCPDS: 33-0268). In other words, a mixture of calcite and vaterite crystals was obtained. The calcite diffraction peaks had a weak intensity while the corresponding main diffraction peaks of vaterite were strong. Using Rietveld refinement quantitative analysis, the calcite and vaterite phase composition was determined to be 36.4% and 63.6%, respectively. The calcite diffraction peaks disappeared upon the application of higher ultrasonic power; all of the XRD peaks belonged to the vaterite form.

The XRD patterns of the products obtained in the presence of the eggshell extract with and without ultrasonic irradiation showed that only vaterite crystals were obtained. Thus, the eggshell extract had a direct effect on the crystal structure and led to the formation of the vaterite phase.

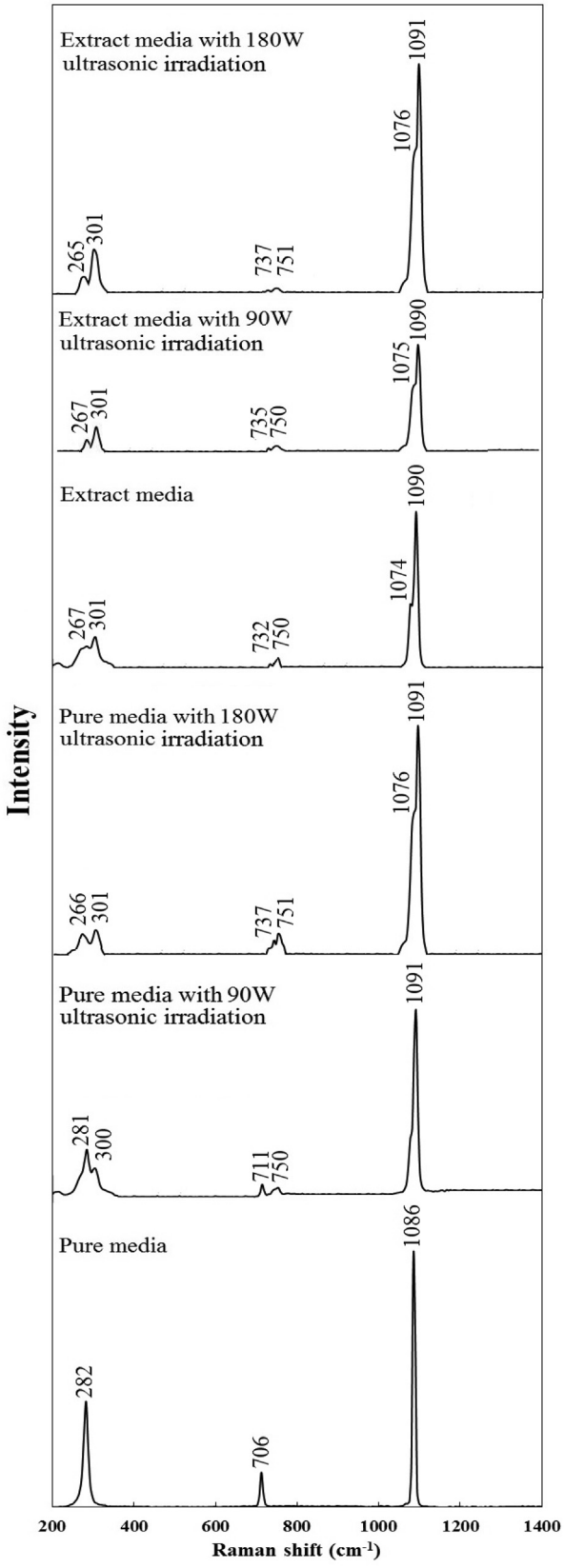


**Fig. 4.** Raman spectra of $CaCO_3$ crystals obtained in pure and eggshell-containing media with and without sonication.

### 3.2. Raman analysis

Raman spectroscopy was applied within a range of 200 to 1400 $cm^{-1}$ to analyze the crystal structure, and the resulting spectra are presented in Fig. 4.

In accordance with the literature [24,25], the Raman spectrum of the crystals obtained in pure media without ultrasonic irradiation exhibited a very strong band centered at 1086 $cm^{-1}$, which was assigned to the internal symmetric stretching mode. The two bands at 282 $cm^{-1}$ and 706 $cm^{-1}$ were assigned to the lattice and in-plane bending modes, respectively.

Ultrasonic irradiation revealed new peaks related to the vaterite form in addition to the calcite peaks. It can be seen in Fig. 4 that there was a mixture of the calcite and vaterite forms in the crystals obtained without eggshell extract at a power of 90 W ultrasonic irradiation, indicating the partial phase transformation of calcite to vaterite, which was also detected by XRD analysis. When the ultrasonic irradiation power was increased to 180 W, the peaks of calcite disappeared and no calcite remained since it had been completely transformed into vaterite. The Raman spectrum of the crystals obtained with 180 W showed two distinct bands at 1076 $cm^{-1}$ and 1091 $cm^{-1}$, which were both assigned to the internal symmetric stretching vibration of the carbonate ions. The peak at 1091 $cm^{-1}$ was stronger than that at 1076 $cm^{-1}$. The two peaks at 266 $cm^{-1}$ and 301 $cm^{-1}$ were attributed to vaterite. Furthermore, the two peaks at 737 $cm^{-1}$ and 751 $cm^{-1}$ were assigned to the in-plane bending mode of vaterite [26].

When the eggshell extract was added to the crystallization medium, regardless of whether ultrasonic irradiation was applied or not, the obtained crystals were in the vaterite form. This shows that the calcite form was fully converted into the vaterite form, which was in line with the XRD results.

### 3.3. FTIR analysis

In order to monitor the polymorphic transformation of $CaCO_3$ crystallization in the presence of eggshell extract, the changes in the crystal polymorphs were also confirmed by ATR-FTIR. Fig. 5 shows the FTIR spectra of $CaCO_3$ crystals obtained in pure and eggshell extract-containing media with and without sonication.

The FTIR spectra clearly indicate that the calcite and vaterite forms have different functional groups. The FTIR spectrum of the crystals obtained in pure media without ultrasonic irradiation shows two peaks at 872 $cm^{-1}$ and 713 $cm^{-1}$, corresponding to the out-of-plane bending and in-plane bending modes of $CO_3^{2-}$, respectively [27]. The crystals obtained in pure media with 90 W ultrasonic irradiation contained peaks for the vaterite form at 1085 $cm^{-1}$ and 742 $cm^{-1}$, while the characteristic peaks of calcite started to disappear [28]. In other words, the mixture of calcite and vaterite forms was observed only in the sample obtained in pure media and treated with the ultrasonic power of 90 W. With the ultrasonic power of 180 W, the calcite peaks disappeared and only vaterite peaks were detected. The same behavior was also observed in the media containing eggshell extract; and only vaterite form $CaCO_3$ crystals were obtained in extract media with and without ultrasonic irradiation.

### 3.4. Morphological analysis

Fig. 6 shows the SEM images of the $CaCO_3$ crystals prepared in pure media and media supplemented with eggshell extract with and without ultrasonication.

The crystals obtained in the pure media without ultrasonic irradiation were in cubic shape, in line with the literature [29,30], and were in calcite form grown over each other and had a tendency to agglomerate. The mean particle size of the crystals was measured as 32 μm with a BET specific surface area of 0.70 $m^2/g$. The SEM images of the $CaCO_3$ crystals obtained in pure media with 90 W ultrasonic

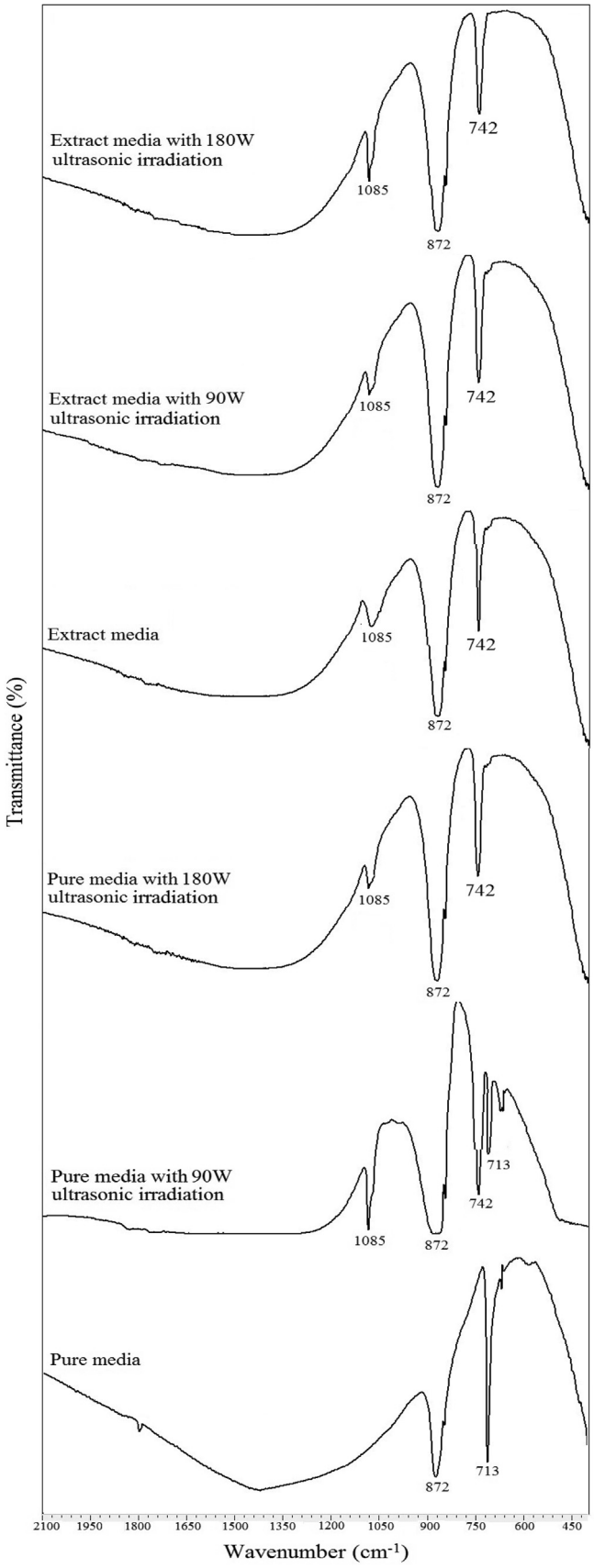


**Fig. 5.** FTIR spectra of $CaCO_3$ crystals obtained in pure and eggshell extract-containing media with and without sonication.

irradiation clearly showed sphere-like vaterite crystals in addition to the cubic calcite crystals. Additionally, the mean particle size of the crystals decreased to 6 μm as a result of the ultrasonication. The BET specific surface area of the crystals that were formed in the ultrasonicated pure medium increased compared to the pure medium without ultrasonication and was measured as 4.12 $m^2/g$. The SEM images of the $CaCO_3$ crystals obtained in pure media with an ultrasonication intensity of 180 W showed that the crystal morphology had completely changed: the cubic form completely disappeared and round plate-structured vaterite crystals were obtained. The specific surface area of the crystals increased to 9.84 $m^2/g$ with the increase of the ultrasonication power.

Fig. 6d displays the SEM image of the $CaCO_3$ crystals obtained in the media containing eggshell extract without ultrasonic power. These crystals had a spherical form with a regular structure and a uniform appearance in the vaterite form. As reported in the literature [31,32], in the absence of additives, calcite's free energy of nucleation is typically lower than that of vaterite. Continually increasing supersaturation will first cause nucleation of calcite. The eggshell extract media can change the nucleation activation energies of calcite and vaterite in the aqueous system, changing the nucleation priority. The formation of vaterite can be attributed to the interaction between the eggshell extract and the calcium and carbonate ions lowering the concentrations of freely available ions in bulk medium and decreasing the thermodynamic driving force for nucleation. A lower nucleation rate delays the formation of more stable calcite polymorphs, thus promoting the formation of the vaterite fraction.

The mean particle size measured as 8 μm for the crystals obtained in the media containing eggshell extract without ultrasonic power. The use of the extract led to a decrease in the mean particle size of the $CaCO_3$ and reduced the tendency for agglomeration observed in the pure media. Additionally, the surfaces of the crystals were shiny and regular and had low porosity. Although the BET surface area slightly increased compared to the crystals obtained in pure media, the obtained value of 1.25 $m^2/g$ is still relatively low. The SEM image of the $CaCO_3$ obtained with the eggshell extract and 90 W ultrasonic irradiation shows spherical vaterite crystals with a cauliflower-like morphology, which emerged as a result of the growth of the crystals as layers.

As the applied ultrasonic intensity was increased, the mean particle size of the $CaCO_3$ crystals decreased and the morphology changed entirely. The regular, round-surfaced crystals were replaced by irregular, rougher crystals with more porous surfaces. The specific surface areas of the crystals in the presence of the eggshell extract were measured as 6.27 and 11.20 $m^2/g$ for 90 W and 180 W ultrasonic power, respectively.

AFM analysis was performed to obtain the surface topography of the $CaCO_3$ obtained in pure and extract-containing media, and the results are presented in Fig. 7.

The topography results for the crystals obtained in pure media shown in Fig. 7a present various levels with a maximum difference of 31.17 nm in thickness. This difference increased with the addition of the eggshell extract to the media. The topography of the $CaCO_3$ crystals obtained in the extract-containing media (Fig. 7b) shows a higher thickness of 54.36 nm, indicating the increase of the surface roughness. Consistent with the SEM images, the $CaCO_3$ obtained in pure media was flat, whilst the use of eggshell extract significantly changed the surface morphology, resulting in an irregular surface topography.

### 3.5. TGA–FTIR analysis

Coupled TGA–FTIR analysis was performed to simultaneously determine the thermal decomposition behavior of $CaCO_3$ obtained in pure and extract media and monitor volatile products evolved during the decomposition process. Fig. 8 shows the thermogravimetric analysis (TG), differential thermogravimetric analysis (DTG), and differential

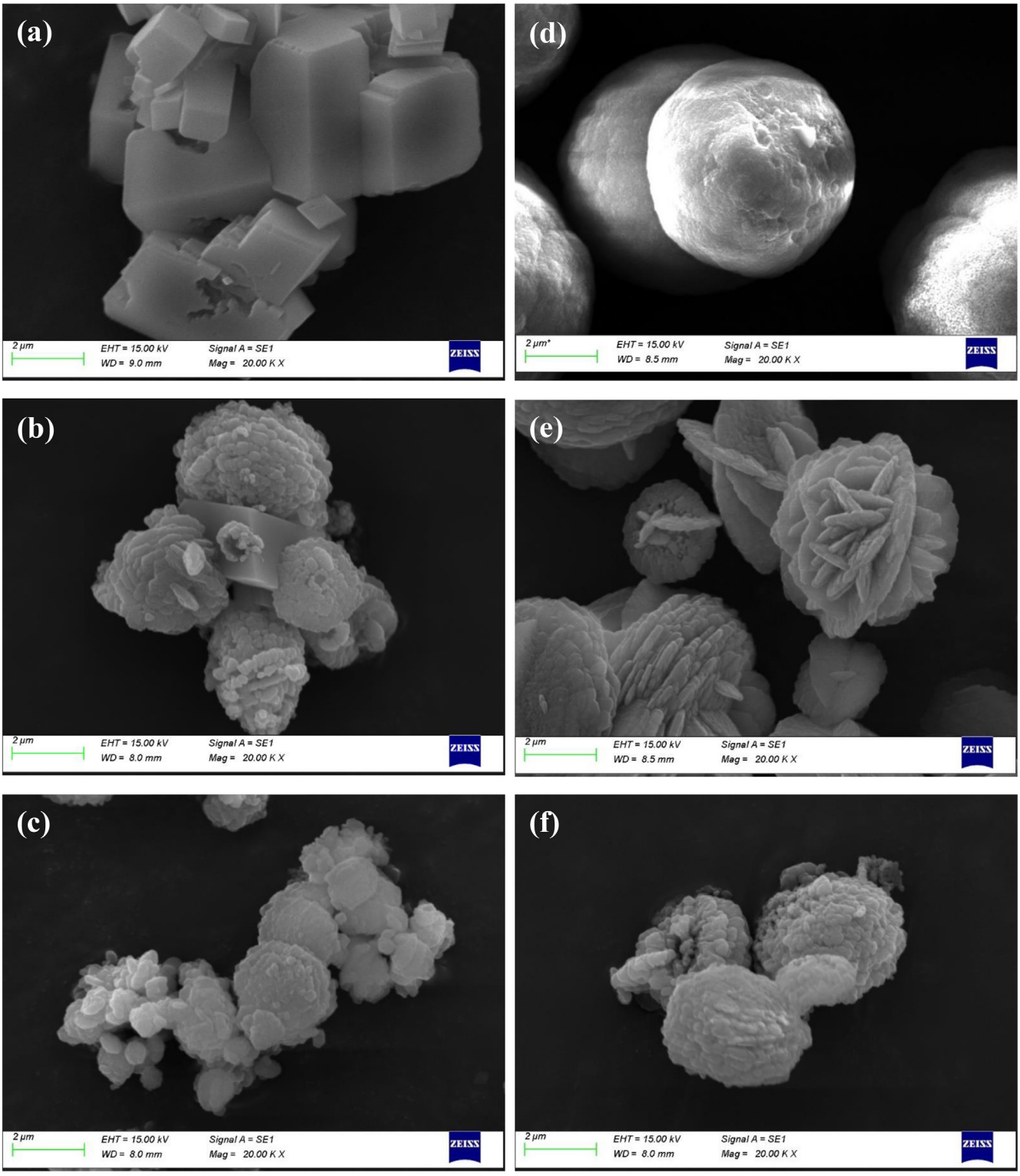


**Fig. 6.** SEM images of $CaCO_3$ crystals obtained in pure media and media supplemented with eggshell extract with and without ultrasonication.

thermal analysis (DTA) plots for $CaCO_3$ obtained in pure and extract-containing media.

From the DTG and DTA curves for the pure and extract media, the peaks at 836.8 °C and 892.5 °C, respectively, correspond to the main weight loss, which was attributed to the transformation of $CaCO_3$ into CaO [33].

From the perspective of the thermal decomposition behavior of the $CaCO_3$ crystals obtained in extract media, which started at approximately 760 °C and ended at 960 °C, the maximum weight loss was observed at 892 °C. Similar to the crystals obtained in pure media, the single peaks in the DTG and DTA plots show that the $CaCO_3$ decomposition occurred in one step. The total weight loss was 44.3 wt% of the initial weight. The addition of the eggshell extract to the crystallization media increased the weight loss rate and shifted the decomposition temperature to a slightly higher value owing to the adsorption of the extract on the $CaCO_3$ surface.

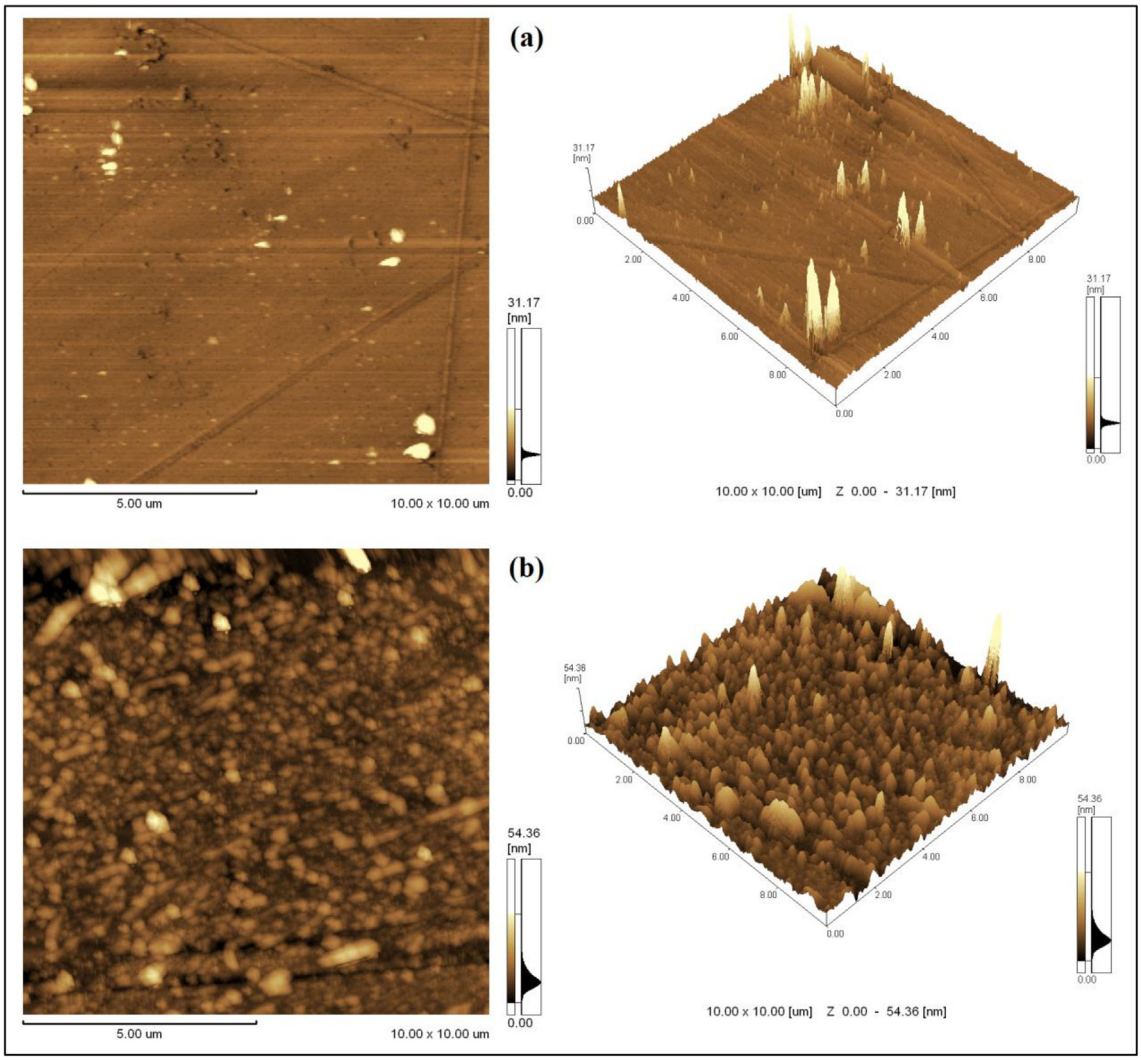


**Fig. 7.** AFM results for $CaCO_3$ crystals obtained in pure (a) and extract-containing media (b).

To further characterize the adsorption of the extract media on the $CaCO_3$ crystals, zeta potential measurements were performed. Zeta potential analysis relates to the surface charge of the particles. The $CaCO_3$ crystals obtained in pure media without ultrasonic irradiation had a zeta potential value of −8.5 mV. The application of ultrasonic irradiation at 90 W and 180 W resulted in positive zeta potential values of 6.6 mV and 9.5 mV, respectively. The addition of eggshell extract to the crystallization media changed the electrical surface charge of the crystals, and their zeta potentials were more negative compared to the crystals obtained in pure media. The crystals obtained in the presence of eggshell extract with no ultrasonication had a zeta potential zeta potential value of −18.4 mV. On the other hand, the zeta potential values were −6.3 mV and −4.4 mV for the $CaCO_3$ crystals obtained with the eggshell extract in the media treated with 90 W and 180 W ultrasonic irradiation. This difference in the zeta potential was attributed to the adsorption of the extract on the $CaCO_3$ surface. In addition to TGA analysis, FTIR analysis was performed simultaneously to gain information about the dynamic evolution of volatiles from the $CaCO_3$ decomposition process. Fig. 9 shows the 3-dimensional (3D) FTIR spectra indicating the individual functional group changes over time for the pure media and eggshell extract-containing media.

As can be seen in both FTIR spectra, the most intense signals for the gaseous products were detected in the 760–960 °C temperature range. The peaks between 2250 and 2500 $cm^{-1}$ and between 580 and 730 $cm^{-1}$ correspond to the stretching and bending vibrations of carbon dioxide, which means that $CO_2$ was the main gas evolved during decomposition and a similar evolution profile was detected in the media with the eggshell extract, but with a distinct increase in the peak intensity. The evolution of carbon dioxide was consistent with the previous thermal decomposition studies performed with $CaCO_3$.

### 3.6. Experimental design results

The response surface methodology (RSM) was used to correlate the relationship among the effects of process variables that influence the BET specific surface area of $CaCO_3$ based on a three-level three-factor Box–Behnken design (BBD). Experimental data were analyzed using the Design Expert 10 statistical software. The individual and combined effects of the process variables (stirring rate, extract concentration, and ultrasonic power) on the BET specific surface area of $CaCO_3$ were analyzed. The range and levels of the variables used in the experimental design are shown in Table 1.

The Box–Behnken matrix, experimental results of the combination of all the factors, and their corresponding responses for each run are given in Table 2.

Based on these results, the model equation as a function of the process variables obtained for the specific surface area (SSA) of $CaCO_3$ crystals can be written as follows:

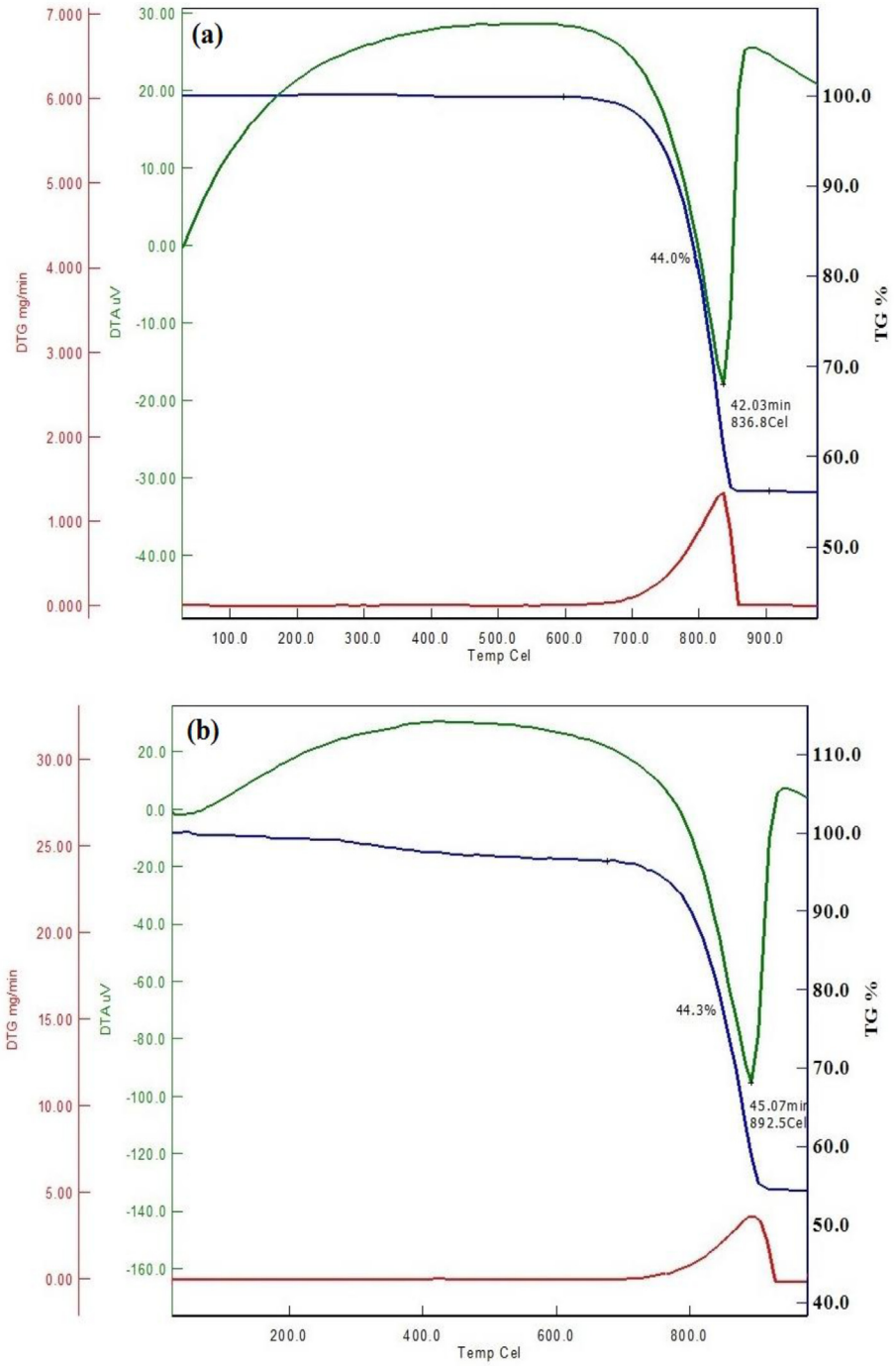


**Fig. 8.** TG, DTG and DTA results for $CaCO_3$ crystals obtained in pure (a) and extract-containing media (b).

$$Y_{SSA} = 6.27 + 0.45A + 0.78B + 4.77C + 0.18AB + 0.27AC + 0.042BC - 0.47A^2 - 0.98B^2 + 0.65C^2 \quad (1)$$

where A is the stirring rate, B is the extract concentration, and C is the ultrasonic power. The highest specific surface area was obtained at 400 rpm, 2.5 wt%, and 180 W. The fit and significance of the model and its coefficient were tested statistically by analysis of variance (ANOVA) [34], the results of which are given in Table 3.

The *p*-value was determined to evaluate the statistical significance of the model. The ANOVA results show a large F value of 228.95 and a small *p*-value $< 0.05$, which verify that the model fit is statistically significant. The precision of the model was checked by the use of the correlation coefficient ($R^2$), which was 0.9976, indicating a good correlation between the measured and predicted responses. The 'Pred $R^2$' value was in reasonable agreement with the "Adj $R^2$" value. Adeq Precision was used to measure the signal to noise ratio, with a value > 4 being desirable. In the present study, the signal to noise ratio was found to be > 4; therefore, the quadratic model could be used to navigate the design space. The independent process variables, stirring rate (A), extract concentration (B), ultrasonic power (C), and the second-order effect of stirring rate ($A^2$), extract concentration ($B^2$), and ultrasonic power ($C^2$) on specific surface area were found to be significant ($p < 0.05$), whereas the other terms were insignificant ($p > 0.1$), as shown in Table 3.

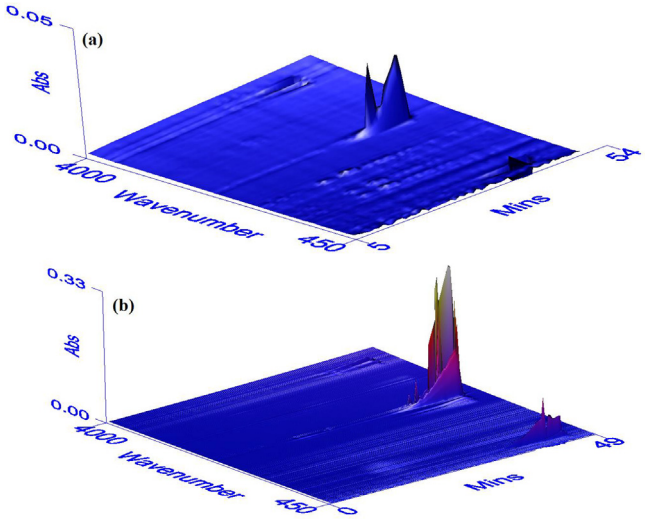


**Fig. 9.** TGA/FTIR results for $CaCO_3$ crystals obtained in pure media (a) and media containing eggshell extract (b).

**Table 1**
Range and levels of the process variables.

| Parameters | Factors | Levels | | |
|---|---|---|---|---|
| | | −1 | 0 | 1 |
| Stirring rate (rpm) | A | 200 | 300 | 400 |
| Extract concentration (wt%) | B | 0 | 2.5 | 5 |
| Ultrasonic power (W) | C | 0 | 90 | 180 |

The relationship between the specific surface area and the combined effect of two variables, namely stirring rate and extract concentration, stirring rate and ultrasonic power, and extract concentration and ultrasonic power at a constant level of the third variable are shown in Fig. 10.

Each plot in Fig. 10 shows the combined effect of two variables on the specific surface area with the third variable fixed. The tendency of each variable studied can be examined by evaluating the response of the surface. Fig. 10 clearly shows that the specific surface of the $CaCO_3$ increased with increasing stirring rate, extract concentration and ultrasonic power. The contour plots are in accordance with the 3D-surface plots. Both the surface and contour plots in Fig. 10 show that a higher surface area was obtained at a higher ultrasonic power. In comparison with the stirring rate and extract concentration, ultrasonic power was the most significant variable affecting specific surface area.

**Table 3**
ANOVA results of the quadratic model for specific surface area.

| Source | Sum of squares | df | Mean square | F-Value | p-value Prob > F |
|---|---|---|---|---|---|
| Model | 195.12 | 9 | 21.68 | 228.95 | < 0.0001 |
| A-Stirring rate | 1.64 | 1 | 1.64 | 17.30 | 0.0088 |
| B-Extract concentration | 4.93 | 1 | 4.93 | 52.06 | 0.0008 |
| C-Ultrasonic power | 181.83 | 1 | 181.23 | 1920.3 | < 0.0001 |
| AB | 0.13 | 1 | 0.13 | 1.41 | 0.2888 |
| AC | 0.30 | 1 | 0.30 | 3.14 | 0.1368 |
| BC | 0.0072 | 1 | 0.0072 | 0.076 | 0.7934 |
| $A^2$ | 0.82 | 1 | 0.82 | 8.66 | 0.0322 |
| $B^2$ | 3.56 | 1 | 3.56 | 37.55 | 0.0017 |
| $C^2$ | 1.58 | 1 | 1.58 | 16.67 | 0.0095 |
| Residual | 0.47 | 5 | 0.47 | | |
| Lack of Fit | 0.47 | 3 | 0.47 | | |
| $R^2$ | 0.9976 | | | | |

Adj R-Squared = 0.9932, Pred R-Squared = 0.9613, Adequate Precision = 45.821, Standard Deviation = 0.31.

## 4. Conclusions

The present study described the polymorphic transformation of $CaCO_3$ in the presence of eggshell extract and ultrasonic irradiation. Firstly, the physicochemical properties of the ground eggshell were determined using XRD and SEM/EDX analysis. Then, the polymorphic transformation of calcite into vaterite was monitored using XRD, Raman, FTIR, SEM, and BET techniques. The results showed that the polymorphic outcome was strongly dependent on both the presence or absence of the eggshell extract and the intensity of the ultrasonic irradiation. The sample obtained without the eggshell extract with 90 W ultrasonic irradiation contained a mixture of calcite and vaterite. An increase in the intensity of ultrasonic irradiation resulted in a sample primarily consisted of the vaterite form with a hexagonal structure. The introduction of the eggshell extract to the crystallization media helped to produce spherical particles with a lower degree of agglomeration and enabled 100% conversion from calcite to vaterite without ultrasonic irradiation. The application of ultrasonic irradiation affected the morphology and size of the $CaCO_3$. The AFM results showed that the $CaCO_3$ crystals produced in the pure media were flat, whilst the crystals formed in the presence of the eggshell extract had an irregular surface topography. Increasing the ultrasonic irradiation intensity and the extract concentration led to an increase in the BET specific surface area. The $CaCO_3$ obtained in eggshell extract media at 180 W ultrasonic irradiation exhibited a BET surface area of 11.20 $m^2/g$. TGA-FTIR analysis identified carbon dioxide as the main gaseous product during $CaCO_3$ decomposition. Furthermore, Box–Behnken design with

**Table 2**
Box–Behnken matrix and experimental results.

| Run | Actual level of factors | | | Coded level of factors | | | Response |
|---|---|---|---|---|---|---|---|
| | Stirring rate (rpm) | Extract concentration | Ultrasonic power (W) | A | B | C | Specific surface area |
| 1 | 300 | 0 | 0 | 0 | −1 | −1 | 0.70 |
| 2 | 300 | 5 | 0 | 0 | +1 | −1 | 1.96 |
| 3 | 300 | 0 | 180 | 0 | −1 | +1 | 9.84 |
| 4 | 300 | 5 | 180 | 0 | +1 | +1 | 11.24 |
| 5 | 200 | 0 | 90 | −1 | −1 | 0 | 3.80 |
| 6 | 200 | 5 | 90 | −1 | +1 | 0 | 5.23 |
| 7 | 400 | 0 | 90 | +1 | −1 | 0 | 4.04 |
| 8 | 400 | 5 | 90 | +1 | +1 | 0 | 6.20 |
| 9 | 200 | 2.5 | 0 | −1 | 0 | −1 | 1.20 |
| 10 | 200 | 2.5 | 180 | −1 | 0 | +1 | 10.50 |
| 11 | 400 | 2.5 | 0 | +1 | 0 | −1 | 1.86 |
| 12 | 400 | 2.5 | 180 | +1 | 0 | +1 | 12.25 |
| 13 | 300 | 2.5 | 90 | 0 | 0 | 0 | 6.27 |
| 14 | 300 | 2.5 | 90 | 0 | 0 | 0 | 6.27 |
| 15 | 300 | 2.5 | 90 | 0 | 0 | 0 | 6.27 |

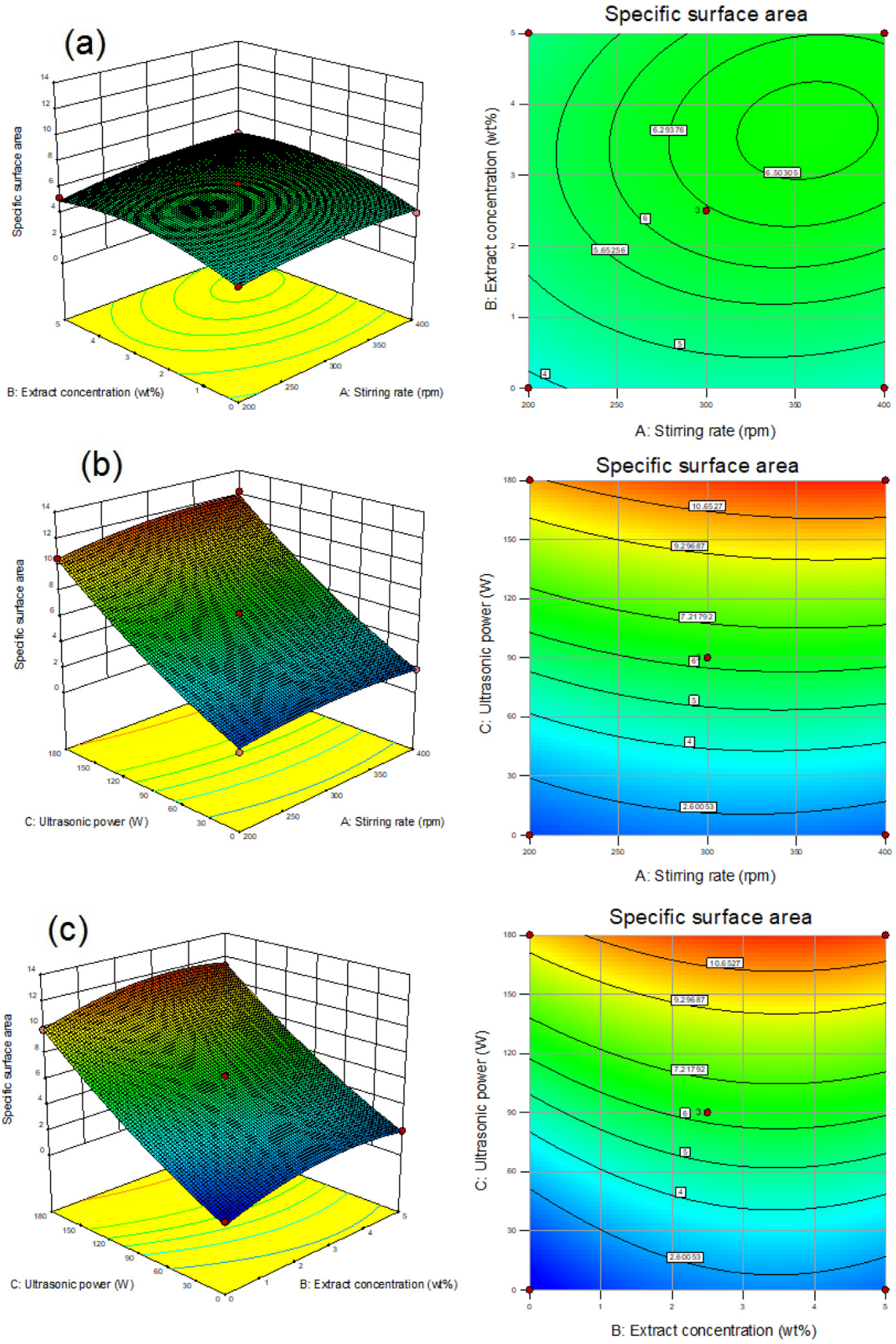


**Fig. 10.** 3D-surface and contour plots showing the effect of (a) stirring rate and extract concentration; (b) stirring rate and ultrasonic power; and (c) extract concentration and ultrasonic power on the specific surface area of $CaCO_3$ crystals.

response surface methodology was used to elucidate the influence of independent variables on the specific surface area of $CaCO_3$. The model equation was established to reveal the relationship between specific surface area and three variables: stirring rate, extract concentration, and ultrasonic power. The model fit well to the experimental data, with an $R^2$ of 0.9976. Among the three investigated variables, ultrasonic irradiation was the most efficient for creating a higher specific surface area. Consequently, it was determined that the combined effects of the extract and ultrasonic irradiation helped to produce better vaterite crystals with higher specific surface area, smaller particle size, and a uniform particle size distribution.

## CRediT authorship contribution statement

**Sevgi Polat:** Conceptualization, Methodology, Investigation, Validation, Formal analysis, Writing - original draft, Writing - review & editing. **Perviz Sayan:** Conceptualization, Methodology, Investigation, Validation, Writing - review & editing, Funding acquisition.

## Declaration of Competing Interest

The authors declare that they have no known competing financial interests or personal relationships that could have appeared to influence the work reported in this paper.

## Acknowledgement

This work was supported by the Marmara University Scientific Research Projects Commission [grant number FEN-A-110718-0396].

## Appendix A. Supplementary data

Supplementary data to this article can be found online at https://doi.org/10.1016/j.ultsonch.2020.105093.

## References

[1] A. Stoica-Guzun, M. Stroescu, S. Jinga, I. Jipa, T. Dobre, L. Dobre, Ultrasound influence upon calcium carbonate precipitation on bacterial cellulose membranes, Ultrason. Sonochem. 19 (4) (2012) 909–915.
[2] X. Zhang, Z. Fan, Q. Lu, Y. Huang, D. Kaplan, H. Zhu, Hierarchical biomineralization of calcium carbonate regulated by silk microspheres, Acta Biomater. 9 (6) (2013) 6974–6980.
[3] M. Fernandes, F.A. Almeida Paz, J.F. Mano, V. de Zea Bermudez, Investigation of calcium carbonate precipitated in the presence of alkanols, Cryst. Res. Technol. 49 (6) (2014) 418–430.
[4] J. Chen, M. Jiang, M. Su, J. Han, S. Li, Q. Wu, Mineralization of calcium carbonate induced by egg substrate and an electric field, Chem. Eng. Technol. 42 (7) (2019) 1525–1532.
[5] Y.W. Wang, Y.Y. Kim, C.J. Stephens, F.C. Meldrum, H.K. Christenson, In situ study of the precipitation and crystallization of amorphous calcium carbonate (ACC), Cryst. Growth Des. 12 (3) (2012) 1212–1217.
[6] H. Cölfen, Precipitation of carbonates: recent progress in controlled production of complex shapes, Curr. Opin. Colloid Interface Sci. 8 (1) (2003) 23–31.
[7] X. Yang, G. Xu, The influence of xanthan on the crystallization of calcium carbonate, J. Cryst. Growth 314 (1) (2011) 231–238.
[8] R.M. Santos, P. Ceulemans, T.V. Gerven, Synthesis of pure aragonite by sonochemical mineral carbonation, Chem. Eng. Res. Des. 90 (6) (2012) 715–725.
[9] L.H. Fu, Y.Y. Dong, M.G. Ma, W. Yue, S.L. Sun, R.C. Sun, Why to synthesize vaterite polymorph of calcium carbonate on the cellulose matrix via sonochemistry process? Ultrason. Sonochem. 20 (5) (2013) 1188–1193.
[10] B. Parakhonskiy, A. Haase, F. Piccoli, I. Caola, F. Tessarolo, T. Bukreeva, R. Antolini, Porous vaterite particles as drug delivery system: synthesis, encapsulation, and controlled release, Eur. Biophys. J. Biophys. Lett. 40 (2011) 230.
[11] R. Schröder, H. Pohlit, T. Schüler, M. Panthöfer, R.E. Unger, H. Frey, W. Tremel, Transformation of vaterite nanoparticles to hydroxycarbonate apatite in a hydrogel scaffold: relevance to bone formation, J. Mater. Chem. B. 3 (2015) 7079–7089.
[12] L. Stajner, J. Kontrec, B.N. Dzakula, N. Maltar-Strmecki, M. Plodinec, D.M. Lyons, D. Kralj, The effect of different amino acids on spontaneous precipitation of calcium carbonate polymorphs, J. Cryst. Growth 486 (2018) 71–81.
[13] K. Naka, S.C. Huang, Y. Chujo, Formation of stable vaterite with poly(acrylic acid) by the delayed addition method, Langmuir 22 (18) (2006) 7760–7767.
[14] M. Mihai, S. Schwarz, F. Doroftei, B.C. Simionescu, Calcium carbonate/polymers microparticles tuned by complementary polyelectrolytes as complex macromolecular templates, Cryst. Growth Des. 14 (2014) 6073–6083.
[15] Y. Sonobe, H. Watamura, I. Hirasawa, Polymorphism, size and shape control of calcium carbonate crystals in the presence of a polyelectrolyte, Chem. Eng. Technol. 38 (6) (2015) 1053–1058.
[16] W. Zhu, J. Lin, C. Cai, Y. Lu, Biomimetic mineralization of calcium carbonate mediated by a polypeptide-based copolymer, J. Mater. Chem. B 1 (2013) 841–849.
[17] M.M. Reddy, A.R. Hoch, Calcite crystal growth rate inhibition by polycarboxylic acids, J. Colloid Interface Sci. 235 (2001) 365–370.
[18] L. Qi, J. Li, J. Ma, Biomimetic morphogenesis of calcium carbonate in mixed solutions of surfactants and double-hydrophilic block copolymers, Adv. Mater. 14 (14) (2002) 300–303.
[19] L. Amer, S. Ouhenia, I. Belabbas, D. Chateigner, The effect of ergocalciferol on the precipitation of calcium carbonate, J. Cryst. Growth 501 (2018) 49–59.
[20] A. Korchef, Effect of iron ions on the crystal growth kinetics and microstructure of calcium carbonate, Cryst. Growth Des. 19 (2019) 6893–6902.
[21] F. Nindiyasari, E. Griesshaber, L. Fernández-Díaz, J.M. Astilleros, N. Sánchez-Pastor, A. Ziegler, W.W. Schmahl, Effects of Mg and hydrogel solid content on the crystallization of calcium carbonate in biomimetic counter-diffusion systems, Cryst. Growth Des. 14 (9) (2014) 4790–4802.
[22] S. Kirboga, M. Oner, E. Akyol, The effect of ultrasonication on calcium carbonate crystallization in the presence of biopolymer, J. Cryst. Growth 401 (2014) 266–270.
[23] Y. Kojima, K. Yamaguchi, N. Nishimiya, Effect of amplitude and frequency of ultrasonic irradiation on morphological characteristics control of calcium carbonate, Ultrason. Sonochem. 19 (4) (2012) 909–915.
[24] A.A. Abalymov, R.A. Verkhovskii, M.V. Novoselova, B.V. Parakhonskiy, D.A. Gorin, A.M. Yashchenok, G.B. Sukhorukov, Live-cell imaging by confocal Raman and fluorescence microscopy recognizes the crystal structure of calcium carbonate particles in HeLa cells, Biotechnol. J. 13 (2018) 1800071 (1–8).
[25] C.G. Kontoyannis, N.V. Vagenas, Calcium carbonate phase analysis using XRD and FT-Raman spectroscopy, Analyst 125 (2000) 251–255.
[26] N. Sánchez-Pastor, A.M. Gigler, J.A. Cruz, S.H. Park, G. Jordan, L. Fernández-Díaz, Growth of calcium carbonate in the presence of Cr(VI), Cryst. Growth Des. 11 (7) (2011) 3081–3089.
[27] K.M. Choi, K. Kuroda, Polymorph control of calcium carbonate on the surface of mesoporous silica, Cryst. Growth Des. 12 (2) (2012) 887–893.
[28] A. Sarkar, S. Mahapatra, Synthesis of all crystalline phases of anhydrous calcium carbonate, Cryst. Growth Des. 10 (5) (2010) 2129–2135.
[29] H. Chen, C. Qing, J. Zheng, Y. Liu, G. Wu, Synthesis of calcium carbonate using extract components of croaker gill as morphology and polymorph adjust control agent, Mater. Sci. Eng. C 63 (2016) 485–488.
[30] Y. Liu, Y. Chen, X. Huang, G. Wu, Biomimetic synthesis of calcium carbonate with different morphologies and polymorphs in the presence of bovine serum albumin and soluble starch, Mater. Sci. Eng. C 79 (2017) 457–464.
[31] W. Hou, Q. Feng, Morphology and formation mechanism of vaterite particles grown in glycine-containing aqueous solutions, Mater. Sci. Eng. C 26 (2006) 644–647.
[32] D.B. Trushina, T.V. Bukreeva, M.V. Kovalchuk, M.N. Antipina, $CaCO_3$ vaterite microparticles for biomedical and personal care applications, Mater. Sci. Eng. C 45 (2014) 644–658.
[33] M.A. Popescu, R. Isopescu, C. Matei, G. Fagarasan, V. Plesu, Thermal decomposition of calcium carbonate polymorphs precipitated in the presence of ammonia and alkylamines, Adv. Powder Techol. 25 (2) (2014) 500–507.
[34] Design-Expert software, Version 10 User's Guide, Stat-Ease.